

Stretchable, Environment-Stable, and Knittable Ionic Conducting Fibers Based on Metallogels for Wearable Wide-Range and Durable Strain Sensors

Qichun Feng, Kening Wan, Tianyi Zhu, Xiaoshan Fan,* Chao Zhang,* and Tianxi Liu*



Cite This: *ACS Appl. Mater. Interfaces* 2022, 14, 4542–4551



Read Online

ACCESS |



Metrics & More

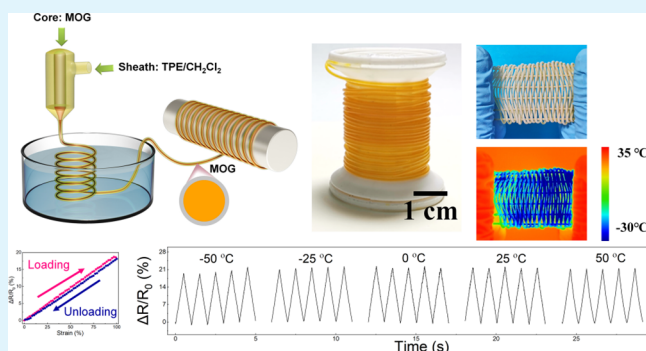


Article Recommendations



Supporting Information

ABSTRACT: The construction of fibrous ionic conductors and sensors with large stretchability, low-temperature tolerance, and environmental stability is highly desired for practical wearable devices yet is challenging. Herein, metallogels (MOGs) with a rapidly reversible force-stimulated sol–gel transition were employed and encapsulated into a hollow thermoplastic elastomer (TPE) microfibrer through a simple coaxial spinning. The resultant MOG@TPE coaxial fiber exhibited a high stretchability (>100%) in a broad temperature range (−50 to 50 °C). The MOG@TPE fibrous strain sensor demonstrated a high-yet-linear working curve, fast response time (<100 ms), highly stable conductivity under large deformation, and excellent cycling stability (>3000 cycles). The MOG@TPE fibrous sensors were demonstrated to be directly attached to the human skin to monitor the real-time movements



of large/facet joints of the elbow, wrist, finger, and knee. It is believed that the present work for preparing the stretchable ionic conductive fibers holds great promise for applications in fibrous wearable sensors with broad temperature range, large stretchability, stable conductivity, and high wearing comfort.

KEYWORDS: ionic conductive fibers, metallogels, force stimulated sol–gel transition, environmental stability, wearable strain sensors

1. INTRODUCTION

Stretchable wearable strain sensors have achieved growing attention in recent years due to a broad range of potential applications including human health monitoring, human–machine interfaces, and soft robotics.^{1–3} Currently, conductive polymer films are commonly employed as stretchable electrodes to assemble stretchable sensors.^{4–7} The resulting sensors exhibit many good properties, such as biocompatibility, real-time monitoring, non-invasive wear, etc.^{8–10} Stretchable conductive fibers as one of the important conductive materials are also exploited for the fabrication of electronic devices.^{11–14} As compared with film-type strain sensors, besides the features ascribed to the stretchable polymers, the sensors based on stretchable conductive fibers show some unique qualities to be directly woven into or stitched onto textiles to detect body motions in the desired direction, further providing wearing comfort and integrality to the resulting wearable sensors.^{15–17} Therefore, stretchable conductive fibers can be considered as ideal candidates to develop high-performance wearable sensors.^{18–20}

To date, various kinds of stretchable conductive fibers with different compositions and architecture have been deliberately designed and fabricated.^{21–23} In general, the methods for the preparation of stretchable conductive fibers can be divided into two categories: (1) spinning the solution of a stretchable

polymer matrix and conductive filler and (2) modifying the polymer yarns and fibers via depositing or printing conductive materials on their surface. Usually, the first method could obtain composite fibers with good filler dispersion and strong interaction between the filler and matrix.²⁴ Moreover, the properties of the resulting fibers could also be readily controlled by tuning the conductive filler amount.^{25,26} However, the conductive fibers fabricated by this method show limited stretchability and long response times, thereby significantly hindering their application in related areas. As for the second method, even though the produced materials exhibit high stretchability, they suffer from the gradual deterioration in conductivity because of the conductive layers delaminating or peeling off from the substrate under repeated stretching, bending, or scratching. So, the development of highly stretchable conductive fibers with stable conductivity is of significance, but it still remains challenging.

Received: November 14, 2021

Accepted: January 5, 2022

Published: January 17, 2022



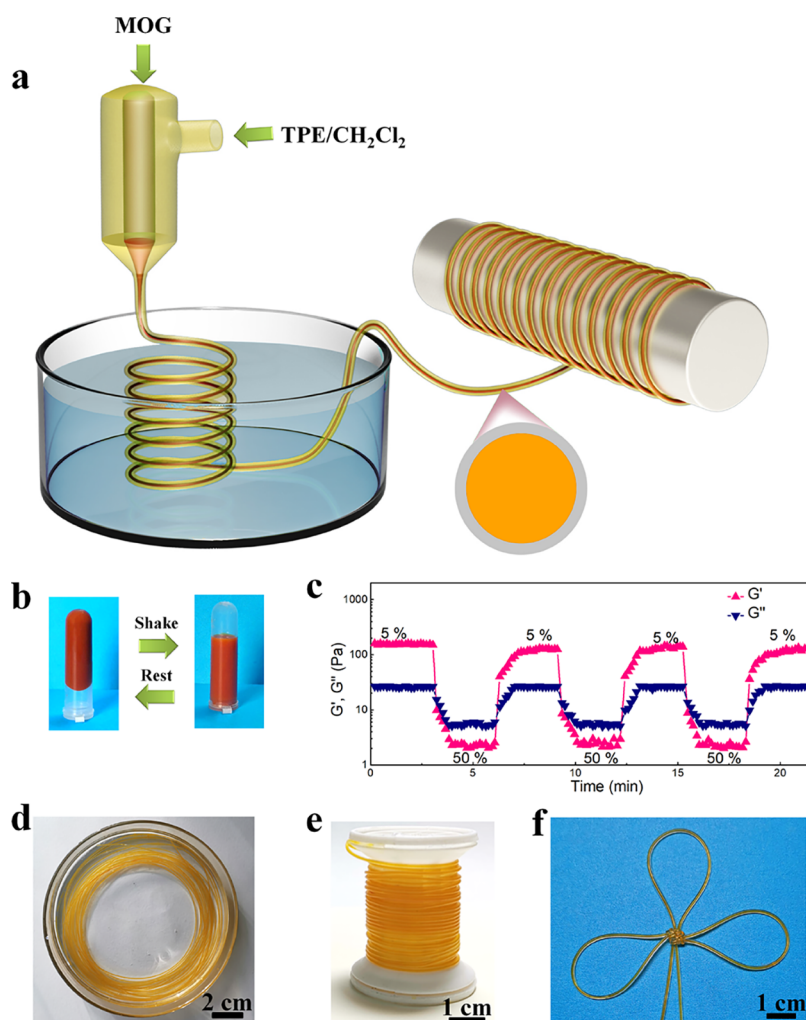


Figure 1. Schematic procedure of the MOG@TPE fiber via coaxial spinning. (a) Schematic illustration of the coaxial spinning for the MOG@TPE fiber. (b) Photograph showing the sol–gel transition behavior of the MOG. (c) Continuous step-stress measurements of the MOG at 5 and 50% strain, respectively. (d) Photograph showing MOG@TPE fibers soaked in EtOH bath. (e) Photograph showing MOG@TPE fibers collected on a spindle. (f) Photograph showing MOG@TPE fibers woven into knots.

Formation of a core–sheath structure via the coaxial spinning technique, wherein the conductive fluids are encapsulated into hollow stretchable polymer fibers, has been proposed as an alternate approach to fabricate hybrid conductive fibers.^{27,28} As compared with the fibers prepared by traditional methods, using a core–sheath structure, it is possible to obtain functional fibers possessing excellent stretchability from the polymer-based sheath and outstanding conductivity of an electroactive core simultaneously.²⁹ A few core–sheath stretchable conductive fibers, such as graphene/chitosan and carbon nanotube/cellulose coaxial fibers, have been designed and prepared by the coaxial spinning of aqueous conductive carbon material suspension and polymer solution.^{30,31} Although the produced fibers exhibit good stretchability, the conductive fillers of graphene sheets or carbon nanotubes have a high tendency to form irreversible aggregation during repeated stretching/releasing processes, which might lead to the unstable conductivity and further limit their applications.

Metallogels (MOGs), emerging as a new kind of functional materials, are one of the supramolecular assemblies through metal–ligand coordination interactions, as well as other weak bonds.^{32–35} One of the MOGs' promising properties is their

good conductivity endowed by their unique compositions.^{36–38} Importantly, non-covalent weak interactions make MOGs readily take reversible sol–gel transition under external stimuli such as shaking, light, pH, and temperature.^{39,40} Herein, we report the facile fabrication of a novel core–sheath conductive fiber for wearable sensor applications in which MOG and thermoplastic TPE have been chosen as the conductive core component and sheath constituent, respectively. The as-prepared fibers exhibit high stretchability benefiting from the good properties of the sheath TPE. Furthermore, they display significantly stable conductivity deriving from the rapidly reversible sol–gel transition of core MOG under shear stress during repeated stretching/releasing processes. In addition, the fibrous strain sensors based on the MOG@TPE fiber are able to directly attach onto the elbow, wrist, finger, and knee to monitor various human movements. The human movements could be easily monitored by the fibrous strain sensors in real time. Overall, the present work provides a new avenue to prepare a MOG-based fibrous strain sensor with broad temperature range, large stretchability, stable conductivity during large deformation, and high wearing comfort.

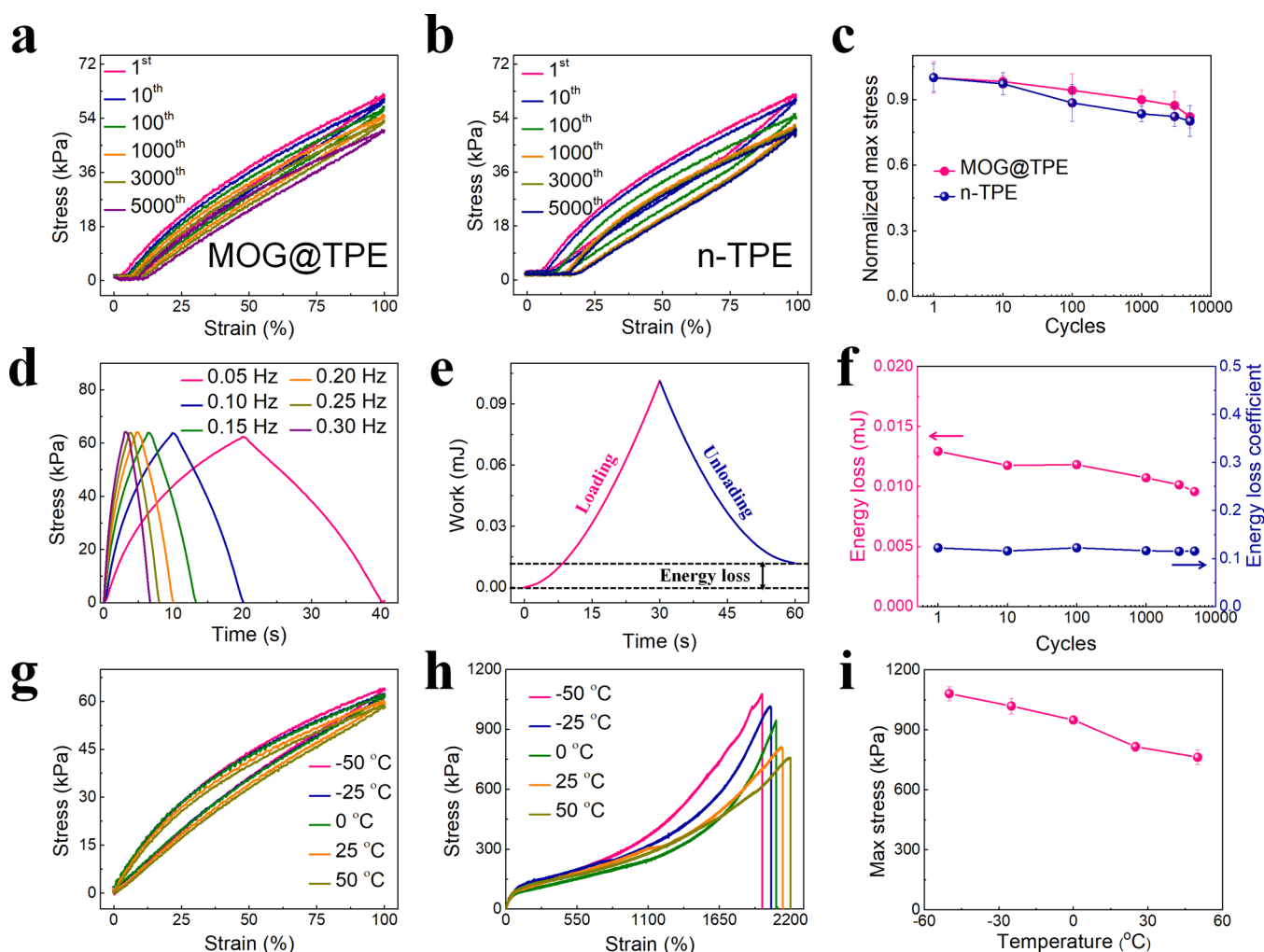


Figure 2. The mechanical properties of the MOG@TPE fiber. (a, b) Cyclic loading and unloading tests on the MOG@TPE fiber (a) and n-TPE fiber (b) from 0 to 100% strain at a rate of 5 cm min⁻¹. (c) Normalized maximum stress of the MOG@TPE fiber and n-TPE fiber, respectively. (d) Time-dependent stress response of the MOG@TPE fiber. (e) Tensile work and energy loss of MOG@TPE fibers at the first cycle. (f) Cycle-dependent energy loss and energy loss coefficient of MOG@TPE fibers. (g) Cyclic loading and unloading tests on the MOG@TPE fiber at various temperatures. (h) Typical strain–stress curves of the MOG@TPE fiber at various temperatures. (i) Fracture mechanical strengths of the MOG@TPE fiber at various temperatures.

2. RESULTS AND DISCUSSION

The fabrication procedure of MOG@TPE fibers is demonstrated in Figure 1a. First, folic acid was dissolved in a solution of KOH containing ethylene glycol and H₂O (EG-H₂O) mixed solvent, and the carboxyl groups (–COOH) on folic acid had a higher coordination activity after losing protons in the KOH solution. Zinc chloride (ZnCl₂) of an equimolar amount with the folic acid was then added to the folic acid solution. Finally, the coordination bonds formed by –COO⁻ and Zn²⁺ offered the MOG skeletons, and EG and H₂O were trapped into the MOG skeletons by hydrogen bonds between the amine groups (–NH₂) and solvent molecules. Since the coordination bonds and hydrogen bonds in the MOG were easy to be broken and regenerated, the MOG had a reversible sol–gel transition behavior (Figure 1b). The reversible sol–gel transition allowed the MOG to be controllably switched between gel and liquid states, which laid the foundation for the successful implementation of the coaxial spinning. The TPE/CH₂Cl₂ solution and MOG were extruded into the coagulation bath from the outer and inner channel, respectively. The CH₂Cl₂ was dissolved into the ethanol, and a hollow TPE fiber tube

was formed quickly. Immediately afterward, the MOG was injected into the hollow TPE fiber tube, and the MOG@TPE fiber was finally obtained by solidifying the as-spun fiber in an oven for 2 days.

Rheology and in situ attenuated total reflectance Fourier transform infrared spectroscopy (ATR-FTIR) were used to study the mechanism of sol–gel transition. A continuous step-strain measurement of the MOG at 5 and 50% strain was used to simulate the shear stress and rest, respectively (Figure 1c).⁴¹ At 5% strain, the values of the storage modulus (G') were constantly higher than those of the loss modulus (G'') ($G' > G''$), indicating that the MOG was in a gel state. When the applied strain increased to 50%, the values of G' were constantly lower than those of G'' ($G' < G''$), indicating that the MOG was in a liquid state. After the applied strain was decreased back to 5%, the gel state was recovered ($G' > G''$) within a few seconds. Furthermore, even after applying the continuous step-strain for three cycles (about 20 min), the MOG can still get back to the gel state, showing that the MOG had excellent sol–gel transition. Figure S1 shows the in situ attenuated total reflectance Fourier transform infrared spec-

trosopy (ATR-FTIR) when the MOG was in the continuous step-strain measurement. The coordination bond ($-\text{COO}^-\text{Zn}^{2+}$) was broken under the applied large strain (50%), evidenced by the intensities of the $-\text{COO}^-\text{Zn}^{2+}$ peak clearly reducing. The intensities of the $-\text{COO}^-\text{Zn}^{2+}$ peak were capable of restoring to original values when the applied strain was decreased to 5%. Herein, the mechanism of sol–gel transition for the MOG was that the shear stress broke the $-\text{COO}^-\text{Zn}^{2+}$ (which transformed the gel state of MOG into the liquid state), and $-\text{COO}^-\text{Zn}^{2+}$ was able to regenerate after resting the liquid state of MOG (Figure S2).⁴²

With the help of the quick sol–gel transition of the MOG, the MOG@TPE fiber can be easily fabricated in an ethanol coagulation bath (Figure 1d), and a single fiber with a length of more than 5 m was collected on a winding shaft (Figure 1e). The outer and inner diameters of MOG@TPE fiber were 600 and 515 μm , respectively (Figure S3). The results showed that the synthetic method in this article holds a potential for the large-scale production of the core–sheath structure conductive fiber. Besides, MOG@TPE fibers showed large stretchability with the strain range of more than 100% strain (Figure S4). A 200 g weight was hung on the MOG@TPE fiber (Figure S5), implying the resultant fiber's excellent mechanical properties. Moreover, MOG@TPE fibers were woven into knots (Figure 1f), indicating that the MOG@TPE fiber had high flexibility and stretchability.

Scanning electron microscope (SEM) images of the xerogel are shown in Figure S6. The xerogel exhibited a three-dimensional (3D) porous network structure with a pore size of 2–3 μm , indicating that the skeletons of the MOG were porous.^{43–45} The changes of functional groups during the formation of the MOG were shown in the Fourier transform infrared spectroscopy (FTIR) of the xerogel and folate dipotassium salt (Figure S7).^{46,47} The peak of $-\text{COO}^-$ (folate dipotassium salt) at 1607 cm^{-1} shifted to 1570 cm^{-1} (xerogel) due to the formation of $-\text{COO}^-\text{Zn}^{2+}$, but the peak of $-\text{NH}_2$ remained at 1509 cm^{-1} during the formation of the MOG. This result indicated the $-\text{COO}^-$ was the only functional group coordinating with Zn^{2+} .^{48–51} In the strain sweep measurements, a linear regime between 1 and 8% can be observed, and the value of G' was higher than that of G'' for the MOG (Figure S8a). In the frequency sweep experiment, a wide range of angular frequencies of 1–100 rad s^{-1} was observed in the linear response of G' and G'' (Figure S8b). The rheological results showed that the elastic characteristics of the MOG were consistent with the related literature, indicating that the gel networks of the MOG had been successfully constructed.^{44,46} To investigate the influence of EG on the gel networks, H_2O -MOG without EG was synthesized. Differential scanning calorimetry (DSC) was used to evaluate the anti-freezing performance of H_2O -MOG and MOG (Figure S9).⁵² A sharp peak near -5°C can be observed on the DSC of H_2O -MOG, indicating that the freezing point of H_2O -MOG was lower than that of pure water, which was attributed to the large amount of Zn^{2+} in H_2O -MOG. However, no peak was observed on the DSC of the MOG, which illustrated that the freezing point of MOG was lower than -75°C . Based on the above results, the mechanism of MOG formation was the $-\text{COO}^-$ coordinating with Zn^{2+} to form the 3D network skeletons, and solvent molecules were trapped into 3D network skeletons by the hydrogen bond (Figure S10).

To investigate the influence of the MOG on the mechanical properties of the MOG@TPE fiber, a neat hollow TPE (n-TPE) fiber was also synthesized. The stress–strain curves of MOG@TPE and n-TPE fibers are shown in Figure 2a,b, respectively. In the first cycle, the maximum stress values of MOG@TPE and n-TPE fibers were similar, which were 61.5 and 61.9 kPa, respectively. The stress–strain curves of Figure 2a show a negligible decrease of the maximum stress for the MOG@TPE fiber in the primary 10 cycles. The fatigue loss of the MOG@TPE fiber was inevitable.⁵³ The maximum stress decrease of the MOG@TPE fiber was up to 6% after 100 cycles and 10% after 1000 cycles. More than that, the MOG@TPE fiber showed a slight maximum stress decrease (13%) after 3000 cycles. As a comparative sample, the maximum stress decrease of the n-TPE fiber was 12% after 100 cycles and 17% after 1000 cycles. The results showed the MOG@TPE fiber had a better fatigue resistance than the n-TPE fiber. The excellent fatigue resistance of the MOG@TPE fiber benefited from the MOG playing the role of lubricant. During the process of stretching, the MOG always remained in the liquid state and effectively avoided the stress concentration of the MOG@TPE fiber. However, the lubrication of MOG was not enough to completely eliminate the stress concentration, and the repeated mechanical tension eventually caused permanent damage to the TPE, i.e., plastic deformation. An 18% decrease of the maximum stress (reaching 50.9 kPa) of the MOG@TPE fiber can be observed after being stretched for 5000 cycles, which was very close to the maximum stress decrease of the n-TPE fiber (20%) after 5000 cycles. Compared with the MOG@TPE fiber, the maximum stress of the n-TPE fiber increased sharply after 10 cycles, and the maximum plastic deformation was reached after 1000 cycles (Figure 2c). This was because there was no MOG as lubricant in the n-TPE fiber, and the stress concentration effect greatly destroyed the microstructure of TPE in the primary 1000 cycles.

The 100% strain was applied on the MOG@TPE fiber at various frequencies (Figure 2d). Each time–stress curve in the results was almost symmetrical, which further showed that the MOG@TPE fiber had highly mechanical properties.^{54–57} The plastic deformation during the stretching process can be quantified as energy dissipation (ΔU), which was the difference between the works of loading and unloading. Taking the first cycle of the MOG@TPE fiber at 100% strain as an example (Figure 2e), the loading work (U) was 0.39 mJ, and the unloading work remained at 0.047 mJ. The energy loss coefficient (η) of the MOG@TPE fiber in the first cycle can be calculated by the following eq 1:

$$\eta = \frac{\Delta U}{U} \quad (1)$$

Therefore, the η of the MOG@TPE fiber was 0.12 in the first cycle, which was attributed to the inevitable microstructure damage caused by stretching the MOG@TPE fiber. After the first cycle, the η did not change significantly and remained at ~ 0.12 (Figure 2f). Specifically, the U was still able to reach 0.31 mJ (Figure S11) after 5000 cycles, indicating that the MOG@TPE fiber had excellent mechanical stretchability.

The effect of temperature on the mechanical properties of the MOG@TPE fiber was also investigated (Figure 2g). Typical stress–strain curves of the MOG@TPE fiber showed the maximum stress slightly increasing with the temperature decreasing, which was attributed to the low temperature restricting the chain motions of TPE. Figure 2h,i shows that

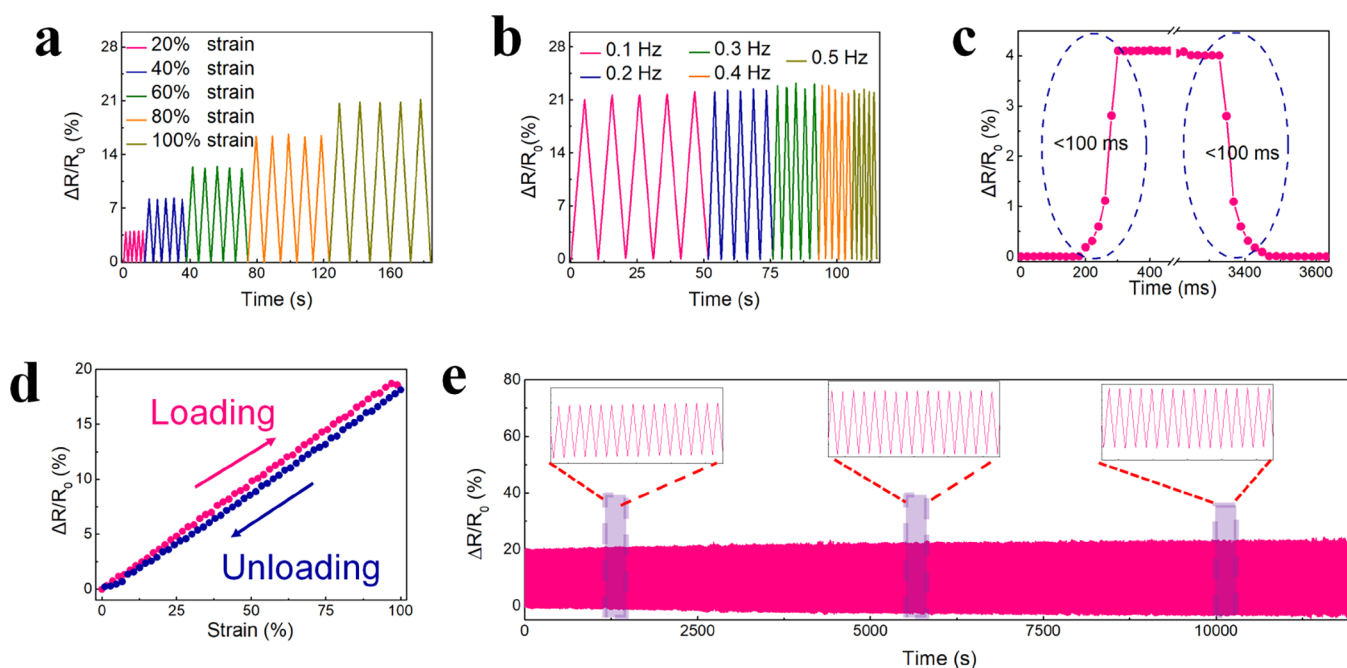


Figure 3. The sensing performance of the MOG@TPE fibrous sensor. Relative resistance variations of the MOG@TPE fibrous sensor at (a) various tensile strains and (b) frequencies, respectively. (c) Response time. (d) Hysteresis performance. (e) Cycling stability of the MOG@TPE fibrous sensor.

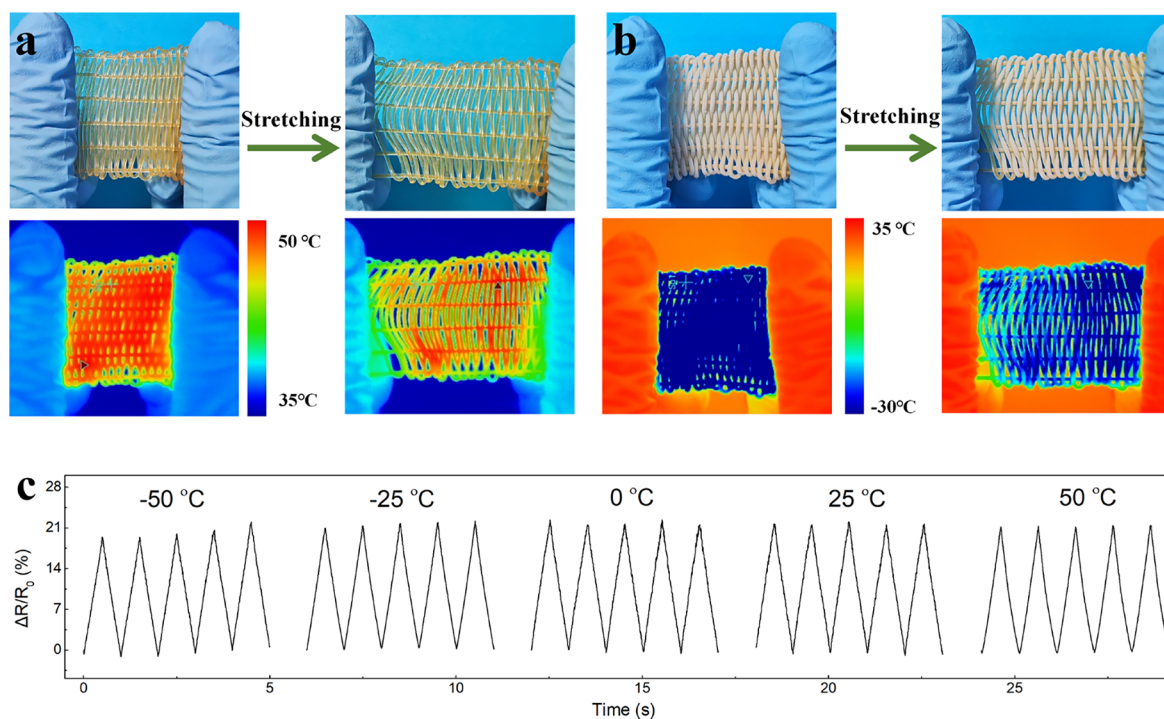


Figure 4. The mechanical properties of the MOG@TPE fiber at different temperatures. (a, b) Photographs showing the bending of a woven fabric of MOG@TPE fibers at $-30\text{ }^\circ\text{C}$ (a) and $50\text{ }^\circ\text{C}$ (b), respectively. (c) Relative resistance variations of MOG@TPE fibrous sensors at various temperatures.

the fracture strength of the MOG@TPE fiber also decreases with rising temperature, but the breaking elongation increases with the temperature rising. The results were mainly attributed to TPE having two different glassy transition temperatures (-60 and $70\text{ }^\circ\text{C}$), which corresponded to the chain motions of isoprene and styrene segments, respectively. It should be pointed out that the MOG had negligible mechanical

properties between -50 and $50\text{ }^\circ\text{C}$. Therefore, low temperatures would induce the TPE into a crystalline state, and the breaking strength of MOG@TPE fiber increased at low temperatures.

A wide strain range is an important characteristic for wearable strain sensors.⁵³ At the frequency of 0.08 Hz , MOG@TPE fibrous sensors based on MOG@TPE fibers were able to

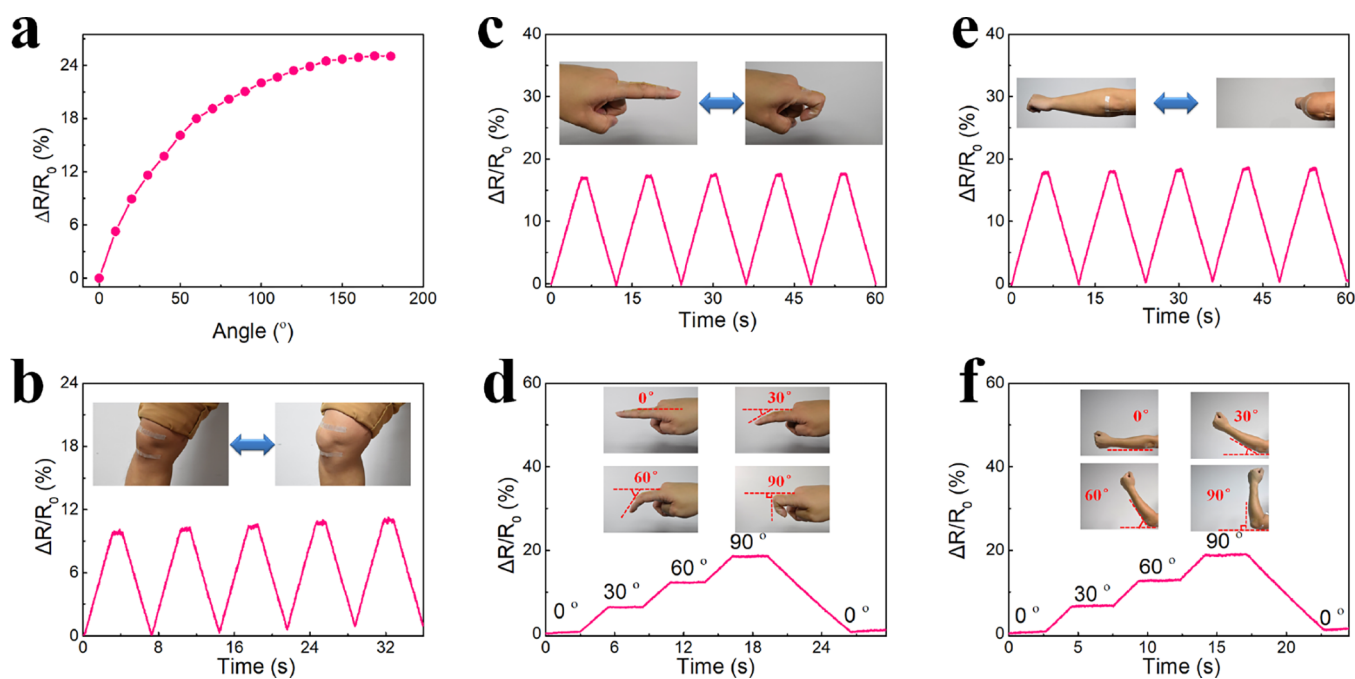


Figure 5. Proof of concept of the MOG@TPE fibrous sensor. The MOG@TPE fibrous sensors monitoring (a) different bending angles, (b) knee bending, (c) figure bending, (d) figure motion of various bending angles, (e) elbow bending, and (f) elbow motion of various bending angles.

output stable and repetitive signals under different strains in the range of 0–100% strain (Figure 3a). When the MOG@TPE fibrous sensor was applied to dynamic tension of 0.1–0.5 Hz under 100% strain (Figure 3b), the output signals of the MOG@TPE fibrous sensor were highly frequency dependent. Figure 3c shows that the response times of tensile and release were all less than 100 ms. The results were attributed to the sheath TPE having few microdefects during wet spinning. Moreover, the resistance signals were very stable before and after stretching. The results were attributed to the fact that the fast and reversible sol–gel transition enabled core MOG in the MOG@TPE fiber to quickly restore to the gel state after stretching. Figure 3d shows that the area enclosed by the curves of loading and unloading was nearly negligible. The results showed that the hysteresis of the MOG@TPE fibrous sensor was very low. The low hysteresis gave MOG@TPE fibrous sensors the ability to output signals quickly. Figure S12 shows that the minimum strain that the MOG@TPE fibrous sensor is capable of detecting is 0.9%, and the $\Delta R/R_0$ of the MOG@TPE fibrous sensor at 0.9% strain is 0.69%.⁵⁸ The MOG@TPE fibrous sensor was stretched repeatedly for 12,000 s (>3000 cycles) at 0.25 Hz, showing that the MOG@TPE fibrous sensor had a long-term working life (Figure 3e). The high repeatable signals presented in the insert of the Figure 3e proved that the MOG@TPE fibrous sensor had high cycling stability.

The effect of temperature on the tensile performance of the fabric woven by MOG@TPE fibers in a harsh environment was studied (Figure 4a,b). The fabric had excellent tensile performance (about 100% strain) at 50 °C (Figure 4a) and –30 °C (Figure 4b). The excellent resistance to extreme temperatures was ascribed to the high anti-freezing performance of EG–H₂O and the great tensile performance of TPE at extreme temperatures. The conductivity of the MOG@TPE fiber was proportional to temperatures (Figure S13). The results were attributed to the fact that the high temperature was able to accelerate the ion migration rate. After 6 months of

storage at various temperatures, the MOG@TPE fiber showed an only 2% weight loss (Figure S14) and had a constant conductivity (Figure S15). The excellent stabilities were ascribed to the fact that the sheath TPE had excellent hydrophobicity and prevented water molecules from entering the MOG@TPE fiber. Figure S16 shows that a slight disturbance was able to accelerate the self-healing speed. The results were attributed to the fact that the contact probability between –COO[–] and Zn²⁺ was increased by the slight disturbance. The quick self-healing performance provided the MOG@TPE fiber resistance to complicated deformations such as stretching and folding. It should be pointed out that the applied strain would partially destroy the coordination networks of the MOG, which in turn makes the metal ions (such as Zn²⁺) restricted in the coordination networks become free, resulting in the resistance decrease (Figures S1 and S2). However, the MOG@TPE fiber would become thin during the stretching process, thus leading to the increase of the resistance. The results demonstrate that the resistance actually increased during the stretching process, meaning that it was mainly affected by the diameter change of the fibers. To further confirm the above-mentioned results, an EG–H₂O solution containing K⁺ and Zn²⁺ free ions, which are the same as the metal ionic concentration in the MOG, was prepared and injected into the TPE hollow fiber tube to obtain a free-ion@TPE fiber. As shown in Figure S17, the resistance change rate of the prepared free-ion@TPE fiber clearly increased during the stretching process with the same strain range, which further confirmed the dependence of the resistance change on the diameter change of the fiber. Figure S18 shows the working curves (0–100% strain) of the MOG@TPE fibrous sensor at –50 to 50 °C. The working curves were similar at various temperatures. More than that, the gauge factor (GF) values (0–100% strain) of the MOG@TPE fibrous sensor were also similar at various temperatures (Figure 4c). The results indicated that the MOG@TPE fiber had the ability to work

stably in a complex environment, which was still a great challenge for traditional fibrous sensors.

The MOG@TPE fibrous sensor was able to monitor different bending angles, indicating that the MOG@TPE fibrous sensor had high sensitivity and broad strain range (Figure 5a). As a proof of concept, MOG@TPE fibrous sensors were attached to human joints as a wearable sensor (the insets in Figure 5b–f). The MOG@TPE fibrous sensor was easy to be worn on humans, and the human skin did not feel discomfort, which showed that the MOG@TPE fibrous sensor had high wearing comfort. Figure 5b shows that the MOG@TPE fibrous sensor was able to monitor the motion of the human knee joint, and a series of real-time simulation curves were obtained. The results show that the MOG@TPE fibrous sensor was able to monitor the motion of large joints. The MOG@TPE fibrous sensor was also capable of simulating the bending and recovery of human fingers (Figure 5c). In addition, the bending angles of the finger can also be accurately monitored in real time by the MOG@TPE fibrous sensor (Figure 5d). The results show that the MOG@TPE fibrous sensor was able to monitor the motion of facet joints. Similarly, the MOG@TPE fibrous sensor was capable of monitoring and accurately simulating different angles of human elbow motion in real time (Figure 5e,f). Figure S19 shows that the MOG@TPE fibrous sensor is also able to monitor human respiration.⁵⁶ In conclusion, the MOG@TPE fibrous sensor had high sensitivity, wide strain range, and excellent wearing comfort.

3. CONCLUSIONS

In summary, coaxial spinning has been successfully used to fabricate a stretchable conductive fiber with a core–sheath structure. The sol–gel transition of core MOG gave the MOG@TPE fiber a stable conductivity (3.6 mS cm^{-1}) after large deformation. Sheath TPE with excellent hydrophobic properties enabled the MOG@TPE fiber to be stored stably for 6 months at various temperatures. The highly mechanical properties of sheath TPE made the MOG@TPE fibrous sensor have a long-term life (12,000 s, >3000 cycles). The mixed solvent of EG–H₂O gave the MOG@TPE fibrous sensor the ability to work stably at various temperatures. As a proof of concept, the MOG@TPE fibrous sensor was able to be worn on human joints, and the large and facet human joints can be accurately and stably monitored in real time by the MOG@TPE fibrous sensor. The present work thus opens a new avenue to fabricate stretchable conductive fibers with broad temperature range, large stretchability, stable conductivity after large deformation, and high wearing comfort.

4. EXPERIMENTAL PROCEDURES

4.1. Materials. Zinc chloride (ZnCl₂, AR), potassium chloride (KCl, AR), ethylene glycol (EG, ≥99.5%), and potassium hydroxide (KOH, ≥90%) were purchased from Sinopharm Chemicals. Folic acid was purchased from Aladdin Chemicals (Shanghai, China). Styrene–isoprene–styrene block copolymer (TPE, styrene 22 wt %), ethanol (≥99.5%), and dichloromethane (CH₂Cl₂, ≥99.5%) were purchased from Sigma-Aldrich. All the chemicals were used as received unless otherwise stated. Deionized (DI) water was used throughout the experiments. All the reagents were used as received without further purification.

4.2. Preparation of the MOG@TPE and Neat TPE Hollow (n-TPE) Fiber. The sheath spinning solution was prepared as follows: 10 g of TPE was dissolved in 20 g of CH₂Cl₂ at room temperature. The folic acid dipotassium salt was prepared as follows: KOH (0.22 g) and

folic acid (0.88 g) were dissolved in 10 mL of DI water. A brown and transparent solution was obtained by stirring the solution at room temperature for 5 min (solution A). Folate dipotassium salt was finally obtained by evaporating the solvent of solution A. The H₂O–MOG was prepared as follows: solution B was obtained by dissolving 0.28 g of ZnCl₂ in 10 mL of H₂O. The H₂O–MOG was obtained after the as-stirred solution (A and B) stood for 2 days at room temperature. The MOG spinning solution was prepared as follows: solution C was obtained by dissolving KOH (0.22 g) and folic acid (0.88 g) in 10 mL of EG–H₂O (volume ratio: 5:5). Solution D was obtained by dissolving 0.28 g of ZnCl₂ in 10 mL of EG–H₂O (volume ratio: 5:5). Then, solutions C and D were mixed by stirring for 5 min. The MOG spinning solution was obtained after the as-stirred solution (C and D) stood for 2 days at room temperature. All the spinning solutions were degassed for 10 min before wet spinning. The coaxial needle was obtained by an inner-channel needle (21G) being inserted into an outer-channel needle (15G). The core MOG and sheath TPE spinning solution was extruded into an ethanol bath from the inner and outer channel, respectively. The MOG@TPE fibers were obtained after the as-spun fiber was washed and air-dried at room temperature. The n-TPE fibers were obtained by extracting the core MOG from the MOG@TPE fibers. The free-ion@TPE fiber was prepared as follows: KCl (0.30 g) and ZnCl₂ (0.28 g) were dissolved in 10 mL of EG–H₂O (volume ratio: 5:5). The free-ion@TPE fiber was obtained by injecting the solution containing free ions into the TPE hollow fiber tube.

■ ASSOCIATED CONTENT

SI Supporting Information

The Supporting Information is available free of charge at <https://pubs.acs.org/doi/10.1021/acsami.1c22099>.

Figures S1–S21: in situ ATR-FTIR of the MOG at different strains; possible mechanism of the MOG in sol–gel transition; cross-sectional photograph of the MOG@TPE fiber; photographs showing MOG@TPE fibers at various strains; photograph showing the MOG@TPE fiber carrying a weight of 200 g; SEM image of the xerogel; FTIR spectra of folic acid dipotassium salt and xerogel; strain sweep rheological curves of MOG, dynamic frequency sweep rheological curves of MOG; DSC curves of MOG and H₂O–MOG; possible structure of the MOG; cycle-dependent *U* of the MOG@TPE fibrous sensor; the minimum strain of the MOG@TPE fibrous sensor; conductivity changes of MOG@TPE fibers at various temperatures; weight changes of MOG@TPE fibers at various temperatures; conductivity changes of MOG@TPE fibers at various temperatures; photograph showing the self-healing process of the MOG; GF values of the MOG@TPE fibrous sensor and free-ion@TPE fiber, respectively; GF values of the MOG@TPE fibrous sensor at various temperatures; the MOG@TPE fibrous sensors monitoring human respiration; schematic images describing how to measure the mechanical properties of MOG@TPE fiber; and schematic images describing how to measure the sensing performance of the MOG@TPE fibrous sensor (PDF)

■ AUTHOR INFORMATION

Corresponding Authors

Xiaoshan Fan – State Key Laboratory for Modification of Chemical Fibers and Polymer Materials, College of Materials Science and Engineering, Donghua University, Shanghai 201620, P.R. China; orcid.org/0000-0002-0617-7400; Email: xsfan@dhu.edu.cn

Chao Zhang – State Key Laboratory for Modification of Chemical Fibers and Polymer Materials, College of Materials Science and Engineering, Donghua University, Shanghai 201620, P.R. China; orcid.org/0000-0003-1255-7183; Email: czhang@dhu.edu.cn

Tianxi Liu – State Key Laboratory for Modification of Chemical Fibers and Polymer Materials, College of Materials Science and Engineering, Donghua University, Shanghai 201620, P.R. China; Key Laboratory of Synthetic and Biological Colloids, Ministry of Education, School of Chemical and Material Engineering, Jiangnan University, Wuxi 214122, P.R. China; orcid.org/0000-0002-5592-7386; Email: txliu@fudan.edu.cn

Authors

Qichun Feng – State Key Laboratory for Modification of Chemical Fibers and Polymer Materials, College of Materials Science and Engineering, Donghua University, Shanghai 201620, P.R. China

Kening Wan – School of Engineering and Materials Science, Queen Mary University of London, London E1 4NS, U.K.

Tianyi Zhu – State Key Laboratory for Modification of Chemical Fibers and Polymer Materials, College of Materials Science and Engineering, Donghua University, Shanghai 201620, P.R. China

Complete contact information is available at:
<https://pubs.acs.org/10.1021/acsami.1c22099>

Author Contributions

The manuscript was written through contributions of all the authors. All the authors have given approval to the final version of the manuscript.

Notes

The authors declare no competing financial interest.

ACKNOWLEDGMENTS

The authors acknowledge the funding support from the Fundamental Research Funds for the Central Universities (2232020G-02) and the National Natural Science Foundation of China (52122303 and 21875033).

REFERENCES

- (1) Wang, W.; Yang, S.; Ding, K.; Jiao, L.; Yan, J.; Zhao, W.; Ma, Y.; Wang, T.; Cheng, B.; Ni, Y. Biomaterials- and Biostructures Inspired High-Performance Flexible Stretchable Strain Sensors: A Review. *Chem. Eng. J.* **2021**, *425*, 129949.
- (2) Jian, M.; Wang, C.; Wang, Q.; Wang, H.; Xia, K.; Yin, Z.; Zhang, M.; Liang, X.; Zhang, Y. Advanced Carbon Materials for Flexible and Wearable Sensors. *Sci. China Mater.* **2017**, *60*, 1026–1062.
- (3) Li, G.; Li, C.; Li, G.; Yu, D.; Song, Z.; Wang, H.; Liu, X.; Liu, H.; Liu, W. Development of Conductive Hydrogels for Fabricating Flexible Strain Sensors. *Small* **2021**, *17*, 2101518.
- (4) He, H.; Zhang, L.; Guan, X.; Cheng, H.; Liu, X.; Yu, S.; Wei, J.; Ouyang, J. Biocompatible Conductive Polymers with High Conductivity and High Stretchability. *ACS Appl. Mater. Interfaces* **2019**, *11*, 26185–26193.
- (5) Fang, Y.; Li, Y.; Li, Y.; Ding, M.; Xie, J.; Hu, B. Solution-Processed Submicron Free-Standing, Conformal, Transparent, Breathable Epidermal Electrodes. *ACS Appl. Mater. Interfaces* **2020**, *12*, 23689–23696.
- (6) Ruan, K.; Shi, X.; Guo, Y.; Gu, J. Interfacial Thermal Resistance in Thermally Conductive Polymer Composites: A Review. *Compos. Commun.* **2020**, *22*, 100518.

(7) Wang, S.; Wang, Z.; Huang, Y.; Hu, Y.; Yuan, L.; Guo, S.; Zheng, L.; Chen, M.; Yang, C.; Zheng, Y.; Qi, J.; Yu, L.; Li, H.; Wang, W.; Ji, D.; Chen, X.; Li, J.; Li, L.; Hu, W. Directly Patterning Conductive Polymer Electrodes on Organic Semiconductor Via in Situ Polymerization in Microchannels for High-Performance Organic Transistors. *ACS Appl. Mater. Interfaces* **2021**, *13*, 17852–17860.

(8) Tan, Z.; Li, H.; Huang, Y.; Gong, X.; Qi, J.; Li, J.; Chen, X.; Ji, D.; Lv, W.; Li, L.; Hu, W. Breathing-Effect Assisted Transferring Large-Area Pdot:Pss to Pdms Substrate with Robust Adhesion for Stable Flexible Pressure Sensor. *Composites, Part A* **2021**, *143*, 106299.

(9) Han, X.; Xiao, G.; Wang, Y.; Chen, X.; Duan, G.; Wu, Y.; Gong, X.; Wang, H. Design and Fabrication of Conductive Polymer Hydrogels and Their Applications in Flexible Supercapacitors. *J. Mater. Chem. A* **2020**, *8*, 23059–23095.

(10) He, G.; Liu, Y.; Gray, D. E.; Othon, J. Conductive Polymer Composites Cathodes for Rechargeable Aqueous Zn-Ion Batteries: A Mini-Review. *Compos. Commun.* **2021**, *27*, 100882.

(11) Zhang, B.; Lei, J.; Qi, D.; Liu, Z.; Wang, Y.; Xiao, G.; Wu, J.; Zhang, W.; Huo, F.; Chen, X. Stretchable Conductive Fibers Based on a Cracking Control Strategy for Wearable Electronics. *Adv. Funct. Mater.* **2018**, *28*, 1801683.

(12) Sun, F.; Tian, M.; Sun, X.; Xu, T.; Liu, X.; Zhu, S.; Zhang, X.; Qu, L. Stretchable Conductive Fibers of Ultrahigh Tensile Strain and Stable Conductance Enabled by a Worm-Shaped Graphene Micro-layer. *Nano Lett.* **2019**, *19*, 6592–6599.

(13) Chen, G.; Wang, H.; Guo, R.; Duan, M.; Zhang, Y.; Liu, J. Superelastic Egain Composite Fibers Sustaining 500% Tensile Strain with Superior Electrical Conductivity for Wearable Electronics. *ACS Appl. Mater. Interfaces* **2020**, *12*, 6112–6118.

(14) Won, C.; Lee, S.; Jung, H. H.; Woo, J.; Yoon, K.; Lee, J.; Kwon, C.; Lee, M.; Han, H.; Mei, Y.; Jang, K.-I.; Lee, T. Ultrasensitive and Stretchable Conductive Fibers Using Percolated Pd Nanoparticle Networks for Multisensing Wearable Electronics: Crack-Based Strain and H2 Sensors. *ACS Appl. Mater. Interfaces* **2020**, *12*, 45243–45253.

(15) Shi, J.; Liu, S.; Zhang, L.; Yang, B.; Shu, L.; Yang, Y.; Ren, M.; Wang, Y.; Chen, J.; Chen, W.; Chai, Y.; Tao, X. Smart Textile-Integrated Microelectronic Systems for Wearable Applications. *Adv. Mater.* **2020**, *32*, 1901958.

(16) Liu, S.; Ma, K.; Yang, B.; Li, H.; Tao, X. Textile Electronics for Vr/Ar Applications. *Adv. Funct. Mater.* **2021**, *31*, 2007254.

(17) Yin, R.; Tao, X.-M.; Xu, B.-g. Yarn and Fabric Properties in a Modified Ring Spinning System Considering the Effect of the Friction Surface of the False-Twister. *Text. Res. J.* **2019**, *90*, 572–580.

(18) Chen, A.; Tan, J.; Henry, P.; Tao, X. The Design and Development of an Illuminated Polymeric Optical Fibre (Pof) Knitted Garment. *J. Text. Inst.* **2020**, *111*, 745–755.

(19) Yang, B.; Xiong, Y.; Ma, K.; Liu, S.; Tao, X. Recent Advances in Wearable Textile-Based Triboelectric Generator Systems for Energy Harvesting from Human Motion. *EcoMat* **2020**, *2*, No. e12054.

(20) Zeng, W.; Shu, L.; Li, Q.; Chen, S.; Wang, F.; Tao, X.-M. Fiber-Based Wearable Electronics: A Review of Materials, Fabrication, Devices, and Applications. *Adv. Mater.* **2014**, *26*, 5310–5336.

(21) Duan, S.; Wang, Z.; Zhang, L.; Liu, J.; Li, C. Three-Dimensional Highly Stretchable Conductors from Elastic Fiber Mat with Conductive Polymer Coating. *ACS Appl. Mater. Interfaces* **2017**, *9*, 30772–30778.

(22) Choi, S.; Yoon, K.; Lee, S.; Lee, H. J.; Lee, J.; Kim, D. W.; Kim, M.-S.; Lee, T.; Pang, C. Conductive Hierarchical Hairy Fibers for Highly Sensitive, Stretchable, and Water-Resistant Multimodal Gesture-Distinguishable Sensor, Vr Applications. *Adv. Funct. Mater.* **2019**, *29*, 1905808.

(23) Cao, Z.; Wang, R.; He, T.; Xu, F.; Sun, J. Interface-Controlled Conductive Fibers for Wearable Strain Sensors and Stretchable Conducting Wires. *ACS Appl. Mater. Interfaces* **2018**, *10*, 14087–14096.

(24) Wang, X.; Liu, X.; Schubert, D. W. Highly Sensitive Ultrathin Flexible Thermoplastic Polyurethane/Carbon Black Fibrous Film

Strain Sensor with Adjustable Scaffold Networks. *Nano-Micro Lett.* **2021**, *13*, 64.

(25) Zhao, Y.; Ren, M.; Shang, Y.; Li, J.; Wang, S.; Zhai, W.; Zheng, G.; Dai, K.; Liu, C.; Shen, C. Ultra-Sensitive and Durable Strain Sensor with Sandwich Structure and Excellent Anti-Interference Ability for Wearable Electronic Skins. *Compos. Sci. Technol.* **2020**, *200*, 108448.

(26) Han, X.; Xiao, W.; Wen, S.; Lin, J.; He, A.; Jiang, Q.; Nie, H. High-Performance Stretchable Strain Sensor Based on Ag Nanoparticles Sandwiched between Two 3d-Printed Polyurethane Fibrous Textiles. *Adv. Electron. Mater.* **2021**, *7*, 2001242.

(27) Tang, X.; Cheng, D.; Ran, J.; Li, D.; He, C.; Bi, S.; Cai, G.; Wang, X. Recent Advances on the Fabrication Methods of Nanocomposite Yarn-Based Strain Sensor. *Nanotechnol. Rev.* **2021**, *10*, 221–236.

(28) Ng, P. F.; Lee, K. I.; Meng, S.; Zhang, J.; Wang, Y.; Fei, B. Wet Spinning of Silk Fibroin-Based Core–Sheath Fibers. *ACS Biomater. Sci. Eng.* **2019**, *5*, 3119–3130.

(29) Li, W.; Zhou, Y.; Wang, Y.; Jiang, L.; Ma, J.; Chen, S.; Zhou, F.-L. Core–Sheath Fiber-Based Wearable Strain Sensor with High Stretchability and Sensitivity for Detecting Human Motion. *Adv. Electron. Mater.* **2021**, *7*, 2000865.

(30) Mirabedini, A.; Foroughi, J.; Thompson, B.; Wallace, G. G. Fabrication of Coaxial Wet-Spun Graphene–Chitosan Biofibers. *Adv. Eng. Mater.* **2016**, *18*, 284–293.

(31) Kou, L.; Huang, T.; Zheng, B.; Han, Y.; Zhao, X.; Gopalsamy, K.; Sun, H.; Gao, C. Coaxial Wet-Spun Yarn Supercapacitors for High-Energy Density and Safe Wearable Electronics. *Nat. Commun.* **2014**, *5*, 3754.

(32) Sebastian, A.; Prasad, E. Cyanide Sensing in Water Using a Copper Metallogel through “Turn-on” Fluorescence. *Langmuir* **2020**, *36*, 10537–10547.

(33) Dietrich, D.; Licht, C.; Nuhnen, A.; Höfert, S.-P.; De Laporte, L.; Janiak, C. Metal–Organic Gels Based on a Bisamide Tetracarboxyl Ligand for Carbon Dioxide, Sulfur Dioxide, and Selective Dye Uptake. *ACS Appl. Mater. Interfaces* **2019**, *11*, 19654–19667.

(34) Malviya, N.; Sonkar, C.; Ganguly, R.; Bhattacharjee, D.; Bhabak, K. P.; Mukhopadhyay, S. Novel Approach to Generate a Self-Deliverable Ru(II)-Based Anticancer Agent in the Self-Reacting Confined Gel Space. *ACS Appl. Mater. Interfaces* **2019**, *11*, 47606–47618.

(35) Chan, M. H.-Y.; Ng, M.; Leung, S. Y.-L.; Lam, W. H.; Yam, V. W.-W. Synthesis of Luminescent Platinum(II) 2,6-Bis(N-Dodecylbenzimidazol-2'-yl)pyridine Foldamers and Their Supramolecular Assembly and Metallogel Formation. *J. Am. Chem. Soc.* **2017**, *139*, 8639–8645.

(36) Saha, E.; Mitra, J. Multistimuli-Responsive Self-Healable and Moldable Nickel(II)-Based Gels for Reversible Gas Adsorption and Palladium Sequestration Via Gel-to-Gel Transformation. *ACS Appl. Mater. Interfaces* **2019**, *11*, 10718–10728.

(37) Tang, S.; Olsen, B. D. Relaxation Processes in Supramolecular Metallogels Based on Histidine–Nickel Coordination Bonds. *Macromolecules* **2016**, *49*, 9163–9175.

(38) Dey, S.; Misra, R.; Saseendran, A.; Pahan, S.; Gopi, H. N. Metal-Coordinated Supramolecular Polymers from the Minimalistic Hybrid Peptide Foldamers. *Angew. Chem., Int. Ed.* **2021**, *60*, 9863–9868.

(39) Guo, J.; Li, Y.; Zhang, Y.; Ren, J.; Yu, X.; Cao, X. Switchable Supramolecular Configurations of Al³⁺/Lystpy Coordination Polymers in a Hydrogel Network Controlled by Ultrasound and Heat. *ACS Appl. Mater. Interfaces* **2021**, *13*, 40079–40087.

(40) Saha, E.; Karthick, K.; Kundu, S.; Mitra, J. Electrocatalytic Oxygen Evolution in Acidic and Alkaline Media by a Multistimuli-Responsive Cobalt(II) Organogel. *ACS Sustainable Chem. Eng.* **2019**, *7*, 16094–16102.

(41) Wang, A.; Wang, Y.; Zhang, B.; Wan, K.; Zhu, J.; Xu, J.; Zhang, C.; Liu, T. Hydrogen-Bonded Network Enables Semi-Interpenetrating Ionic Conductive Hydrogels with High Stretchability and Excellent

Fatigue Resistance for Capacitive/Resistive Bimodal Sensors. *Chem. Eng. J.* **2021**, *411*, 128506.

(42) Wang, Y.; Liu, Y.; Plamthottam, R.; Tebyetekerwa, M.; Xu, J.; Zhu, J.; Zhang, C.; Liu, T. Highly Stretchable and Reconfigurable Ionogels with Unprecedented Thermoplasticity and Ultrafast Self-Healability Enabled by Gradient-Responsive Networks. *Macromolecules* **2021**, *54*, 3832–3844.

(43) Wei, J.; Liao, M.; Ma, A.; Chen, Y.; Duan, Z.; Hou, X.; Li, M.; Jiang, N.; Yu, J. Enhanced Thermal Conductivity of Polydimethylsiloxane Composites with Carbon Fiber. *Compos. Commun.* **2020**, *17*, 141–146.

(44) Guo, H.; Feng, Q.; Xu, K.; Xu, J.; Zhu, J.; Zhang, C.; Liu, T. Self-Templated Conversion of Metallogel into Heterostructured Tmp@Carbon Quasiaerogels Boosting Bifunctional Electrocatalysis. *Adv. Funct. Mater.* **2019**, *29*, 1903660.

(45) Guo, H.; Zhou, J.; Li, Q.; Li, Y.; Zong, W.; Zhu, J.; Xu, J.; Zhang, C.; Liu, T. Emerging Dual-Channel Transition-Metal-Oxide Quasiaerogels by Self-Embedded Templating. *Adv. Funct. Mater.* **2020**, *30*, 2000024.

(46) Sun, Y.; Chen, C.; Liu, J.; Stang, P. J. Recent Developments in the Construction and Applications of Platinum-Based Metallacycles and Metallacages Via Coordination. *Chem. Soc. Rev.* **2020**, *49*, 3889–3919.

(47) Wang, Y.; Wang, K.; Zhang, C.; Zhu, J.; Xu, J.; Liu, T. Solvent-Exchange Strategy toward Aqueous Dispersible MoS₂ Nanosheets and Their Nitrogen-Rich Carbon Sphere Nanocomposites for Efficient Lithium/Sodium Ion Storage. *Small* **2019**, *15*, 1903816.

(48) Yu, Q.; Zheng, Y.; Wang, Y.; Shen, L.; Wang, H.; Zheng, Y.; He, N.; Li, Q. Highly Selective Adsorption of Phosphate by Pyromellitic Acid Intercalated ZnL-Ldhs: Assembling Hydrogen Bond Acceptor Sites. *Chem. Eng. J.* **2015**, *260*, 809–817.

(49) Yang, R. G.; Wang, M. L.; Liu, T.; Zhong, G. Q. Room Temperature Solid State Synthesis, Characterization, and Application of a Zinc Complex with Pyromellitic Acid. *Crystals* **2018**, *8*, 56.

(50) Luo, Y.; Yang, Q.; Nie, W.; Yao, Q.; Zhang, Z.; Lu, Z. H. Anchoring Irpdau Nanoparticles on Nh₂-Sba-15 for Fast Hydrogen Production from Formic Acid at Room Temperature. *ACS Appl. Mater. Interfaces* **2020**, *12*, 8082–8090.

(51) Chatterjee, S.; Paital, A. R. Functionalized Cubic Mesoporous Silica as a Non-Chemodosimetric Fluorescence Probe and Adsorbent for Selective Detection and Removal of Bisulfite Anions Along with Toxic Metal Ions. *Adv. Funct. Mater.* **2018**, *28*, 1704726.

(52) Zhang, B.; Zhang, X.; Wan, K.; Zhu, J.; Xu, J.; Zhang, C.; Liu, T. Dense Hydrogen-Bonding Network Boosts Ionic Conductive Hydrogels with Extremely High Toughness, Rapid Self-Recovery and Autonomous Adhesion for Human-Motion Detection. *Research* **2021**, *2021*, 9761625.

(53) Shi, P.; Wang, Y.; Tjiu, W. W.; Zhang, C.; Liu, T. Highly Stretchable, Fast Self-Healing, and Waterproof Fluorinated Copolymer Ionogels with Selectively Enriched Ionic Liquids for Human-Motion Detection. *ACS Appl. Mater. Interfaces* **2021**, *13*, 49358–49368.

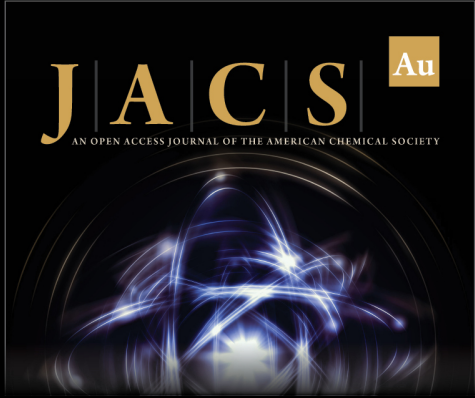
(54) Qin, M.; Xu, Y.; Cao, R.; Feng, W.; Chen, L. Efficiently Controlling the 3d Thermal Conductivity of a Polymer Nanocomposite Via a Hyperelastic Double-Continuous Network of Graphene and Sponge. *Adv. Funct. Mater.* **2018**, *28*, 1805053.

(55) Zhang, F.; Feng, Y.; Qin, M.; Gao, L.; Li, Z.; Zhao, F.; Zhang, Z.; Lv, F.; Feng, W. Stress Controllability in Thermal and Electrical Conductivity of 3d Elastic Graphene-Crosslinked Carbon Nanotube Sponge/Polyimide Nanocomposite. *Adv. Funct. Mater.* **2019**, *29*, 1901383.


(56) Wang, Y.; Tebyetekerwa, M.; Liu, Y.; Wang, M.; Zhu, J.; Xu, J.; Zhang, C.; Liu, T. Extremely Stretchable and Healable Ionic Conductive Hydrogels Fabricated by Surface Competitive Coordination for Human-Motion Detection. *Chem. Eng. J.* **2021**, 127637.

(57) Yu, X.; Zheng, Y.; Zhang, H.; Wang, Y.; Fan, X.; Liu, T. Fast-Recoverable, Self-Healable, and Adhesive Nanocomposite Hydrogel Consisting of Hybrid Nanoparticles for Ultrasensitive Strain and Pressure Sensing. *Chem. Mater.* **2021**, *33*, 6146–6157.


(58) Li, C.; Zhang, D.; Deng, C.; Wang, P.; Hu, Y.; Bin, Y.; Fan, Z.; Pan, L. High Performance Strain Sensor Based on Buckypaper for Full-Range Detection of Human Motions. *Nanoscale* **2018**, *10*, 14966–14975.




JACS Au
AN OPEN ACCESS JOURNAL OF THE AMERICAN CHEMICAL SOCIETY



Editor-in-Chief
Prof. Christopher W. Jones
Georgia Institute of Technology, USA

Open for Submissions 

pubs.acs.org/jacsau  ACS Publications
Most Trusted. Most Cited. Most Read.